ACS APPLIED MATERIALS & INTERFACES

Research Article

www.acsami.org

Terthiophene-Containing Copolymers and Homopolymer Blends as High-Performance Dielectric Materials

Md. Sayful Islam,[†] Yali Qiao,[‡] Chuanbing Tang,[‡] and Harry J. Ploehn*,[†]

[†]Department of Chemical Engineering and [‡]Department of Chemistry and Biochemistry, University of South Carolina, Columbia, South Carolina 29208, United States

Supporting Information

ABSTRACT: This work explores the dielectric and polarization properties of block copolymers and homopolymer blends containing a terthiophene-rich, electronically polarized block (PTTEMA) and an insulating polystyrene block (PS). PTTEMA-*b*-PS block copolymers were synthesized by reverse addition−fragmentation chain transfer (RAFT) polymerization, and PTTEMA/PS homopolymer blends with the same PTTEMA weight percentages were produced by solution blending. DSC and XRD characterization show that crystallinity increases with PTTEMA content, indicating the presence of terthiophene-rich crystalline domains. Under an applied electric field, these domains are electronically polarized, but the insulating PS block inhibits current leakage, resulting in enhanced dielectric properties. Impedance measurements show that relative permittivity increases with PTTEMA content. The permittivity values are higher in PTTEMA-*b*-PS copolymers with moderate PTTEMA content due to the ability of the PS block to inhibit PTTEMA association, resulting in a higher density of isolated, terthiophene-rich polarizable domains. Freestanding PTTEMA/PS blend films containing up to 40 wt % PTTEMA have almost 40% greater recoverable energy density compared to pure PS films polarized to the same electric field strength.

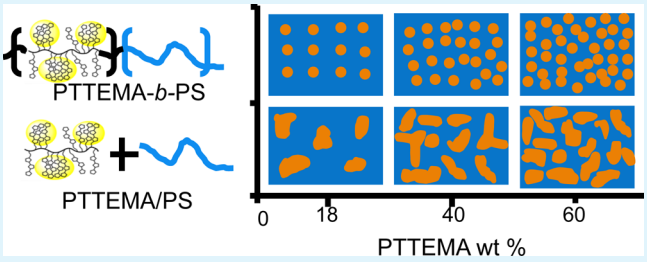

KEYWORDS: *terthiophene, copolymer, polymer blend, dielectrics, impedance, permittivity, polarization, energy density*

1. INTRODUCTION

High-performance dielectric materials are needed for both commercial and military purposes.[1−4] All applications need energy storage devices with high energy and power density, low dissipation, and/or very high rate capability ("pulse power"). Power conditioning systems need to handle power pulses with rise times of less than 1 ms and AC power at frequencies ranging from kilohertz to megahertz. However, the limiting factor for large capacitors ($C > 1$ F) is low energy density, which results in devices that occupy too much volume. One of the best practical dielectric capacitor materials available today, metalized, biaxially oriented polypropylene (BOPP), has a volumetric energy density of about 1.7 J/cm^3 (as packaged).[5] This magnitude of energy density does not solve the volume occupancy issue for large electric systems for pulse power and power conditioning operations. Thus, new dielectric materials with higher volumetric energy density are needed to advance the development of compact capacitors for commercial power electronics and transportation applications.

Inorganic/organic polymer composites for dielectric applications have been reviewed previously.[1,6−10] In many cases, poor compatibility between the inorganic fillers and the organic polymer matrix leads to aggregation and defects, resulting in high dielectric loss, reduced breakdown strength, and suboptimal stored energy density. To address these issues, a variety of "all-polymer" approaches have been explored.[11] Most attention has been focused on high ε_r polymers such as polyvinylidiene fluoride (PVDF), related copolymers,[1,12−18] and their blends.[19−25] In general, blends involving PVDF and related fluorine-containing copolymers produce high ε_r values, but the dielectric losses are high as well.[19−26] Polymer blending studies involving PVDF-based polymers with non-fluorine-containing polymers[19,21,22,25] aim to reduce dielectric loss but with only limited success.[21]

Another all-polymer approach explores percolative dielectric composites[26−33] prepared by dispersing conductive organic domains in an insulating polymer matrix. Charge migration in the conducting organic domains results in space charge accumulation at the interface between the conducting and the insulating domains. In effect, the conducting domains become "super-dipoles" with large dipole moments, high polarization density, and thus a high effective dielectric constant. As the volume fraction of the organic conductor domain increases, ε_r reaches a maximum value at just below the percolation threshold. Compared with inorganic−organic composites, all-organic percolative dielectric composites offer advantages such as facile processability, lighter weight, and possibly lower cost. Problems with this approach include undesirable macrophase separation, excessive leakage current, and low breakdown field strength.

Received: November 6, 2014
Accepted: December 31, 2014
Published: December 31, 2014

DOI: 10.1021/am507751m
ACS Appl. Mater. Interfaces 2015, 7, 1967−1977

Scheme 1. RAFT Polymerization Synthesis of Homopolymer PTTEMA$_m$ and Block Copolymer PTTEMA$_m$-*b*-PS$_{in}$

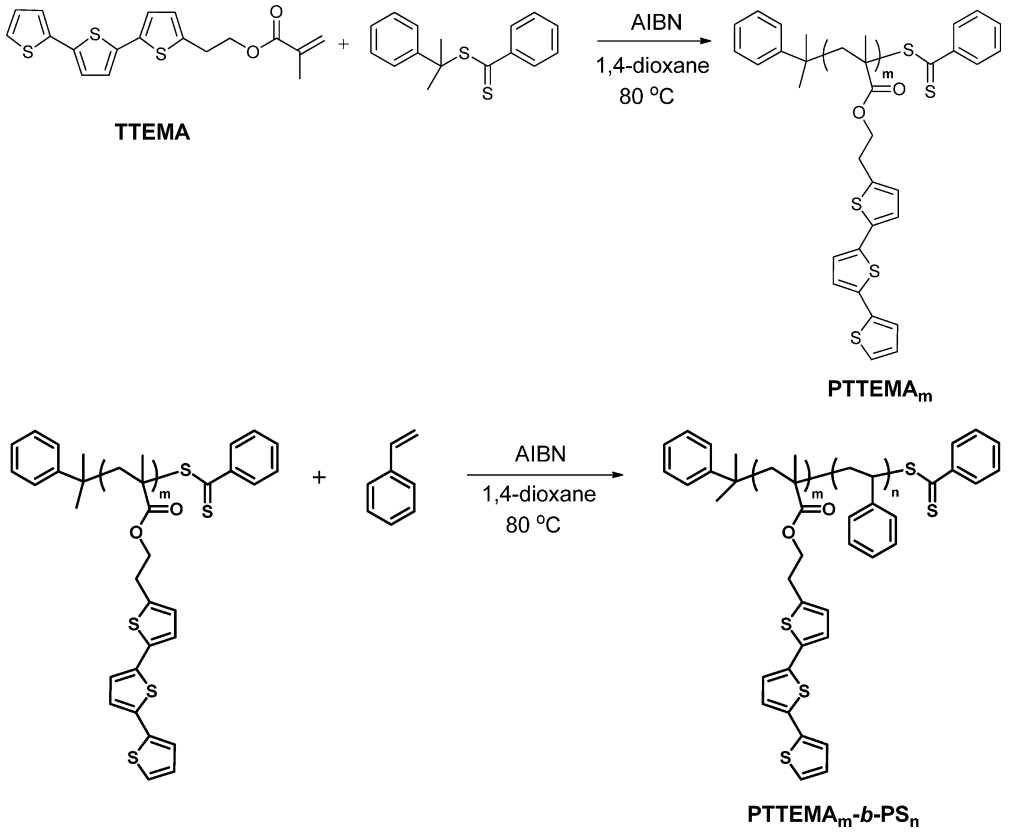

Block copolymer dielectrics[34−38] go beyond this concept by taking advantage of the covalent bonding between two (or more) dissimilar polymer blocks. Like all-polymer percolative composites, this approach develops interfacially−dominated dielectric materials that store energy through electronic conduction and interfacial polarization. The block copolymer molecular architecture features conductive and insulating blocks. The conducting block forms nanoscale domains with high electronic conductivity, while the other block insulates the conducting domains to prevent percolation and interdomain conduction. Under an applied electric field, electronic conduction results in space charge accumulation and local dipole formation along the boundaries between the conducting and the insulating domains. As the conducting domain size decreases, the interfacial area between the domains increases, resulting in dielectric materials with energy storage dominated by interfacial polarization. It is expected that this method will circumvent the limitations of existing polymer dielectrics to meet requirements for next-generation polymer dielectrics for pulse power and power conditioning applications.

Early work on this concept explored the synthesis and properties of polystyrene (PS) end capped with conducting oligoaniline blocks.[34,35,39] Although these materials exhibited higher ε_r values than pure PS, doping oligoaniline with acid to make it conductive resulted in ionic charge migration and excessive dielectric loss. Subsequent efforts began to investigate polymers incorporating thiophene-containing monomers to produce electronically conducting blocks without the need for acid doping. Specifically, we synthesized terthiophene ethyl methacrylate (TTEMA) monomer and carried out RAFT polymerization to produce PTTEMA.[38] In simple terms, this polymer features an insulating ethyl methacrylate backbone with pendant terthiophene side groups. Wide-angle XRD indicates the existence of nanoscale domains (~2 nm) resulting from association of terthiophene groups on neighboring PTTEMA chains. PTTEMA films have high dielectric constant and low loss (ε_r > 10 and tan δ < 0.02), nearly independent of field frequency from 1.0 kHz to more than 1.0 MHz. Nearly linear polarization (D−E) curves resulted in recoverable energy density values up to 1.5 J/cm^3 with polarization losses of 8% or less.

Although PTTEMA homopolymers offer very promising dielectric properties, film samples were brittle and thus difficult to handle. Moreover, the homopolymer architecture does not permit the exploration of composition variables that might shed additional light on structure−property relationships. The present work reports the synthesis and dielectric properties of PTTEMA-*b*-PS block copolymers as well as PTTEMA/PS homopolymer blends. The goal is to gain a better understanding of the factors governing polarization behavior in terthiophene-containing polymers.

We address two questions. First, which aspect dominates dielectric performance: do nanoscale crystalline domains play a role in enhancing dielectric properties or is the presence of terthiophene in the polymer architecture sufficient? Second, does the block copolymer architecture of PTTEMA-*b*-PS offer any advantage compared to PTTEMA/PS homopolymer blends? To answer these questions we prepared PTTEMA-*b*-PS block copolymers and PTTEMA/PS blends with varying PTTEMA wt %, characterized crystalline structure via XRD, and characterized dielectric properties via low-voltage impedance spectroscopy and high-voltage polarization measurements.

DOI: 10.1021/am507751m
ACS Appl. Mater. Interfaces 2015, 7, 1967−1977

2. EXPERIMENTAL PROCEDURES

2.1. Materials. All reagents were purchased from Alfa Aesar and Sigma-Aldrich and used as received unless otherwise noted. 1,4-Dioxane was dried over 4 Å molecular sieves for 24 h and distilled before use. The synthesis of monomer 2-([2,2′:5′,2″-terthiophen]-5-yl)ethyl methacrylate (TTEMA) and preparation of homopolymer PTTEMA by reversible addition−fragmentation chain transfer (RAFT) have been described previously.[38]

2.2. Synthesis of PTTEMA-*b*-PS Block Copolymers. *PTTEMA-Macroinitiator.* Following our previous report,[38] cumyl dithiobenzoate (0.06 g, 0.22 mmol), TTEMA (8 g, 22.19 mmol), AIBN (0.01 g, 0.067 mmol), and 22.1 mL of dry 1,4-dioxane were added to a 50 mL Schlenk flask and degassed by 5 cycles of freeze−pump−thaw. An initial sample was taken before the flask was submerged into an 80 °C preheated oil bath to initiate RAFT polymerization (Scheme 1). Samples were taken out at predetermined intervals to monitor the reaction conversion by ^{1}H NMR before stopping the reaction. When conversion reached about 58%, the reaction flask was immediately cooled in an ice bath and the mixture was diluted with tetrahydrofuran. The terthiophene-containing polymer was purified by precipitation into cold hexane three times to remove any unreacted TTEMA monomers and vacuum dried at room temperature, resulting in a light yellow powder (yield 4.35 g, 54%). The degree of polymerization was determined from conversion monitored by ^{1}H NMR (DP = 58). M_n 12 200 g mol^{-1} (GPC), $Đ$ 1.18 (GPC). M_n 20 900 g mol^{-1} (conversion monitored by ^{1} H NMR). ^{1}H NMR (300 MHz, $CDCl_3$, δ (ppm)): 7.67−7.84 (broad, Ph from RAFT agent end group), 6.50−7.25 (m, aromatic proton from terthiophene side chain), 4.10 (s, $-CH_2O-$), 2.96 (s, $-CH_2$ in side chain), 1.76−2.10 (m, $-CH_2$ in polymer backbone), 0.71−1.01 (m, $-CH_3$). A sufficient quantity of $PTTEMA_{58}$ was prepared so that the same polymer product could be used for synthesis of all PTTEMA-*b*-PS block copolymers and PTTEMA/PS homopolymer blends.

PTTEMA-b-PS Diblock Copolymers. Since RAFT is a "living" controlled radical polymerization, the $PTTEMA_{58}$ block serves as the macroinitiator for further chain extension with styrene to form the diblock copolymer PTTEMA-*b*-PS. A specified ratio of styrene, macroinitiator PTTEMA, and AIBN (e.g., for $PTTEMA_{58}$-*b*-PS_{136}, [St]:[PTTEMA]:[AIBN] = 335:1:0.2) was dissolved in dry 1,4-dioxane, added to a 10 mL Schlenk flask, and degassed by 5 cycles of freeze−pump−thaw. An initial sample was taken before the flask was submerged into an 80 °C preheated oil bath to continue RAFT polymerization of the block copolymer (Scheme 1). Samples were taken out at predetermined intervals to monitor the reaction conversion by ^{1}H NMR. When conversion reached a target value (e.g., for $PTTEMA_{58}$-*b*-PS_{136}, target conversion is ca. 40%), the reaction flask was immediately cooled in an ice bath and the mixture was diluted with tetrahydrofuran. The terthiophene-containing block polymer was purified by precipitation into cold hexane three times to remove any unreacted styrene and vacuum dried at room temperature, resulting in a light yellow powder product. The degree of polymerization for PS was determined by conversion monitored by ^{1}H NMR (e.g., for $PTTEMA_{58}$-*b*-PS_{136}, DP = 136 for PS calculated from conversion ca. 40%). All diblock copolymer samples were characterized by GPC to determine their M_n and $Đ$. All of the corresponding integral peaks from each block could be exactly assigned in ^{1}H NMR spectra. The results confirmed the successful synthesis of PTTEMA-*b*-PS block copolymers.

2.3. Preparation of PTTEMA and PS Blends. Blends of PTTEMA and PS homopolymers were prepared by solution blending. First, PS was added to THF (typically about 0.03 g/mL) and sonicated for 3−4 h until completely dissolved. Next, a measured amount of PTTEMA homopolymer was added to the solution and sonicated for another 2−3 h. The blend solutions were then used to prepare films. We prepared a series of PTTEMA/PS blends with PTTEMA weight percentages corresponding to the wt % PTTEMA in PTTEMA-*b*-PS block copolymers. Although the PTTEMA and PS weight fractions in the physical blends and copolymers are equal, we recognize that the blends are based on a single high MW PS, while the PS blocks in the copolymers have varying molecular weights.

2.4. Film Sample Preparation. Films for impedance spectroscopy and polarization measurements were prepared by solution casting using THF. PTTEMA/PS homopolymers and PTTEMA-*b*-PS copolymers were dissolved in THF (10 mg/mL) and sonicated for 2−3 h. The resultant solutions were poured into clean heavy-gauge aluminum pans. The THF was removed by evaporation at 44 °C under reduced pressure (635 mmHg absolute) for about 3 h without any post-treatment (thermal annealing). This resulted in films with uniform thickness and minimal incidence of bubbles, cracks, or other defects (Figures S1 and S2, Supporting Information). Film thicknesses were measured at multiple positions with a micrometer and found to be in the 3−15 μm range. Strips of aluminum pan bearing dried polymer films were cut using scissors. The aluminum pan served as the bottom electrode for dielectric measurements. Gold was sputter coated under argon atmosphere through a shadow mask to deposit circular gold electrodes (area 1.13 cm^2) on the films' top surfaces.

Most of the PTTEMA/PS blend films spontaneously peeled away from the Al pan. In these cases, gold electrodes were sputtered on both sides of the freestanding films. We have not observed any significant variations in dielectric properties due to variations in electrodes.

2.5. Characterization Methods. ^{1}H NMR (300 MHz) spectra were collected on a Varian Mercury 300 spectrometer with tetramethylsilane (TMS) as an internal reference. Gel permeation chromatography (GPC) was carried out on a Varian system equipped with a Varian 356-LC refractive index detector and a Prostar 210 pump. The columns were STYRAGEL HR1 and HR2 (300 × 7.5 mm) from Waters. HPLC-grade DMF with 0.01 wt (%) LiBr was used as an eluent with a flow of 1.0 mL/min. Polystyrene standards were used for GPC calibration.

Differential scanning calorimetry (DSC, TA Instruments DSC-Q200) characterized thermal transitions of hermetically sealed, 10 mg samples. The first heating/cooling scan ramped the temperature at a rate of 10 °C/min (under N_2 purge per ASTM D3418) up to 200 °C and then down to 0 °C. The second heating scan ramped the temperature from 0 to 240 °C. To avoid inaccuracy due to variable thermal history, comparisons use DSC data from the first cooling and the second heating cycle. The DSC instrument software automatically extracts melting and crystallization enthalpy values from the peaks in the heating and cooling curves.

Wide-angle X-ray diffraction (WXRD) employed a powder diffractometer (Rigaku D/Max 2100) using Cu Kα radiation (λ = 1.5419 Å). Scattered intensity data were recorded from 2° to 60° (2θ) at a rate of 0.5° per minute and a step resolution of 0.02°.

The complex impedance of copolymer and polymer blend film samples was measured using an impedance analyzer (Agilent model 4192A LF). Measurements were carried out at a fixed applied voltage (10 mV) and varying frequency (typically from 10^2 to 1.2×10^7 Hz). Impedance spectra were collected for 3−5 specimens of each sample to ensure reproducibility; average values are reported. The real and complex parts of the impedance, expressed as impedance magnitude and phase angle, were analyzed using a parallel RC circuit model describing a "leaky" capacitor, yielding values of relative permittivity (ε_{eff}) and loss tangent (tan δ) as functions of frequency.

Polarization measurements at higher applied voltages employed a polarization tester (Precision Multiferroic, Radiant, Inc.). Polarization data (D versus E) were obtained for applied voltages up to 2000 V with a cycle frequency of 1.0 kHz. The maximum applied field strength depended on the sample film thickness and breakdown strength. Stored energy density ($\hat{W}_s$) was determined by numerical integration of E, according to $\hat{W} = \int E\,dD$, from $D = 0$ to the maximum value of D (D_{max}) achieved in the hysteresis loop. Recovered energy density ($\hat{W}_r$) was determined by numerically integrating E from D_{max} to the value of D where $E = 0$. Percentage energy loss is computed as $100 \times (\hat{W}_s - \hat{W}_r)/\hat{W}_s$.

DOI: 10.1021/am507751m
ACS Appl. Mater. Interfaces 2015, 7, 1967−1977

3. RESULTS AND DISCUSSION

3.1. Polymer Characterization. Starting with the same $PTTEMA_{58}$ macroinitiator, a series of block copolymers with varying PS weight fraction were synthesized (Table 1). Figure 1

Table 1. Molecular Weight Information for PS, PTTEMA, and PTTEMA-*b*-PS Block Copolymers

polymer	PTTEMA M_n, (DP) (g/mol)	PS M_n, (DP) (g/mol)	PDI (GPC)	TTEMA wt %
PS	n.a.	192 000 (1850)[a]	*a*	0
$PTTEMA_{58}$-*b*-PS_{901}	20 900 (58)	93 700 (901)	1.22	18
$PTTEMA_{58}$-*b*-PS_{304}	20 900 (58)	31 600 (304)	1.29	40
$PTTEMA_{58}$-*b*-PS_{136}	20 900 (58)	14 100 (136)	1.28	60
$PTTEMA_{58}$	20 900 (58)	n.a.	1.18	100

[a] M_n for PS used in blends obtained from vendor information. DP was calculated from M_n; PDI is unknown.

shows a representative ^{1}H NMR spectrum for $PTTEMA_{58}$-*b*-PS_{136}; additional spectra for $PTTEMA_{58}$ and other PTTEMA-*b*-PS block copolymers may be found in the Supporting Information (Figures S3–S5). The monomer conversion from ^{1}H NMR was used to calculate the degree of polymerization and number-average molecular weight (M_n) for PTTEMA and PTTEMA-*b*-PS block copolymers. GPC traces (Figure S6, Supporting Information) show distinct shifts from the $PTTEMA_{58}$ macroinitiator to PTTEMA-*b*-PS block copolymers, with the elution volume clearly decreasing as the DP of the PS block increases. The clarity of the peak shifts and absence of secondary peaks at low MW shows that all $PTTEMA_{58}$ macroinitiator molecules participated in the chain-extension reaction. Dispersities ($Đ$) of all block polymers were in the range from 1.22 to 1.29, indicating narrow molecular weight distributions.

3.2. Thermal Properties and Crystalline Structure. Differential scanning calorimetry (DSC) and wide-angle X-ray diffraction (WXRD) measurements were performed to characterize the crystalline microstructure of PTTEMA-*b*-PS copolymers and PTTEMA/PS blends. Figure 2 shows DSC heating and cooling curves for PTTEMA and PS homopolymers, PTTEMA-*b*-PS copolymers, and PTTEMA/PS blends. The heating curve for PTTEMA homopolymer (Figure 2a) shows an endothermic peak at T_m = 137.3 °C due to crystallite melting, in agreement with previous results[38] for $PTTEMA_{61}$. The heating curves for the copolymers all show endothermic peaks in the 135–137 °C range (values in Table 2). Likewise, cooling curves for PTTEMA homopolymer and PTTEMA-*b*-PS copolymers all manifest sharp exothermic peaks in the 109–111 °C (T_c) range due to crystallization. These results demonstrate the presence of PTTEMA crystallites in the PTTEMA-*b*-PS copolymers.

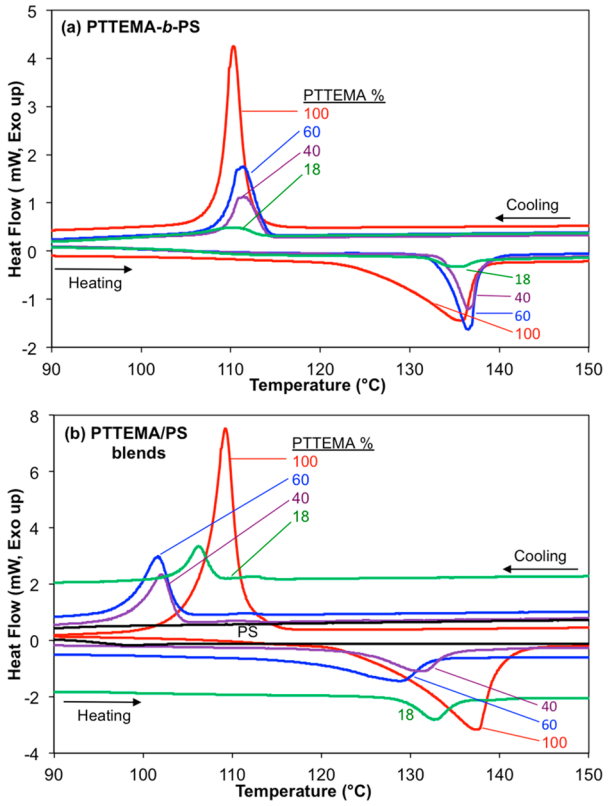

Figure 2. DSC heat flow curves for (a) $PTTEMA_{58}$ homopolymer and PTTEMA-*b*-PS block copolymers, and (b) PS homopolymer and PTTEMA/PS polymer blends.

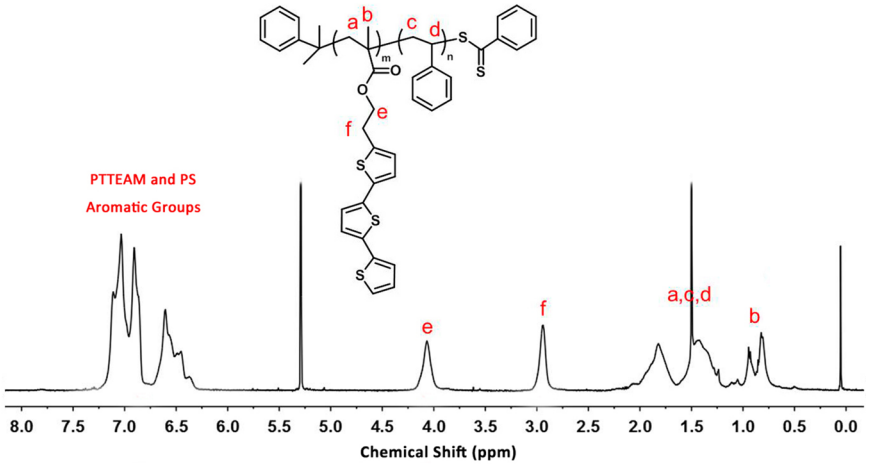

Figure 1. ^{1}H NMR spectrum of $PTTEMA_{58}$-*b*-PS_{136} block copolymer. Peaks labeled a–f on the spectrum correspond to the protons associated with the carbon atoms labeled a–f on the $PTTEMA_{58}$-*b*-PS_{136} molecular structure.

DOI: 10.1021/am507751m
ACS Appl. Mater. Interfaces 2015, 7, 1967–1977

Table 2. Thermal Properties of PTTEMA Homopolymer, PTTEMA-*b*-PS Copolymers, and PTTEMA/PS Blends

	T_m (°C)	$-\Delta H_m$ (J/g)	T_c (°C)	ΔH_c (J/g)
PTTEMA homopolymer and PTTEMA-*b*-PS block copolymers				
PTTEMA	137.3	16.7	109.2	17.4
60% PTTEMA	136.5	7.9	111.4	8.0
40% PTTEMA	136.5	4.9	111.5	4.6
18% PTTEMA	135.3	1.3	109.6	2.0
PTTEMA/PS blends				
60% PTTEMA	128.7	8.3	101.7	9.7
40% PTTEMA	131.2	4.3	102.1	5.2
18% PTTEMA	133.0	1.9	106.2	2.2

Because T_m and T_c do not depend on PTTEMA wt %, crystallization in PTTEMA-*b*-PS copolymers does not depend on the PS block MW. However, the enthalpies of crystallite melting ($-\Delta H_{cm}$) and crystallization (ΔH_c) clearly increase with PTTEMA wt % (Table 2 and Figure 3). Thus,

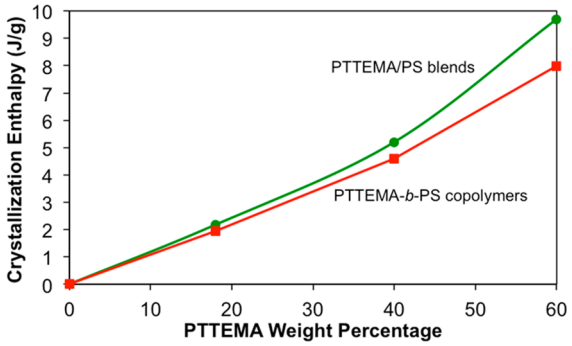

Figure 3. Crystallization enthalpy (ΔH_c) as a function of PTTEMA wt % for PTTEMA-*b*-PS block copolymers and PTTEMA/PS blends.

crystallization in PTTEMA-*b*-PS primarily involves the PTTEMA block, likely due to association of terthiophene side groups in PTTEMA-rich crystalline domains, just as in PTTEMA homopolymers.[38] The quantity of these domains increases with PTTEMA wt %.

The PTTEMA/PS polymer blends (Figure 2b) exhibit distinct crystallization and melting transitions, but the pure PS does not. Crystallization in PTTEMA/PS blends is probably associated with the PTTEMA component, since it is unlikely that PTTEMA nucleates crystallization in PS. In the blends, the crystallite melting during heating occurs at temperatures (T_c) 4−9 °C lower than that of PTTEMA homopolymer. During cooling, crystallization in PTTEMA/PS blends occurs at temperatures 3−8 °C lower than in PTTEMA homopolymer. This suggests that the presence of high-MW PS alters the kinetics of the melting and crystallization processes in the PTTEMA component. However, the enthalpies of crystallite melting and crystallization in the blends ($-\Delta H_m$ and $-\Delta H_c$, Table 2 and Figure 3) are proportional to PTTEMA wt %, as found for the block copolymers. This implies that crystallization in PTTEMA/PS blends primarily involves the PTTEMA component.[38] At the same PTTEMA wt %, the blend has a crystallization enthalpy ($-\Delta H_c$) greater than that of the corresponding copolymer (Table 2 and Figure 3) on unit mass basis. This implies that the crystallinity of PTTEMA in PTTEMA/PS blends is marginally greater than that in PTTEMA-*b*-PS. This may be rationalized in terms of the greater configurational freedom of PTTEMA in the blends compared to the block copolymers.

Figure 4 shows XRD patterns for PTTEMA and PS homopolymers, PTTEMA-*b*-PS copolymers, and PTTEMA/PS blends. Considering the homopolymers first, the pattern for $PTTEMA_{58}$ agrees well with that reported previously[38] for $PTTEMA_{61}$. The sharpness of the main peak, its asymmetry, and its breadth at the base suggest it represents superposition of diffraction from both amorphous and crystalline domains. Deconvolution of the data produces several overlapping peaks, with the sharpest component (centered at 2θ = 18.9°) attributed to crystalline domains formed by nanoscale association of terthiophene side chains.[38] Using the Scherrer formula,[40−43] the estimated size of these domains in $PTTEMA_{58}$ is about 1.65 nm, comparable to the 1.82 nm value reported for $PTTEMA_{61}$.[38] The remaining deconvoluted broad peaks are attributed to the amorphous halo associated with PTTEMA's methacrylate backbone, which is very similar to that observed for amorphous poly(methyl methacrylate).[38] The commercial PS homopolymer used in this work is atactic and amorphous. Its XRD pattern agrees well with that reported previously[44,45] and consists entirely of an amorphous halo with broad peaks centered at 2θ = 8.4° and 19.1°.

The XRD patterns for PTTEMA-*b*-PS copolymers (Figure 4) display features that vary with the relative sizes of the PTTEMA and PS blocks. The shapes of the main peaks for $PTTEMA_{58}$-*b*-PS_{136} (60% PTTEMA) and $PTTEMA_{58}$-*b*-PS_{304} (40% PTTEMA) are similar to that of $PTTEMA_{58}$ homopolymer, as are the shapes of the peaks extracted via deconvolution. As PS fraction increases, a shoulder appears near 2θ = 10° in the pattern for $PTTEMA_{58}$-*b*-PS_{304}, becoming a distinct secondary peak for $PTTEMA_{58}$-*b*-PS_{901} (18% PTTEMA). These observations indicate the increasing contribution of the PS amorphous halo to the block copolymers' XRD pattern as the PS block size and wt % increase.

Unfortunately, the peak attributed to PTTEMA terthiophene domains nearly coincides with a PS amorphous halo peak at approximately 2θ = 19°. For this reason, we do not use the Scherrer equation to extract a crystallite size from this peak or interpret it in terms of the terthiophene domain size. Nonetheless, the peak shapes for the copolymers with larger PTTEMA weight fractions suggest the presence of crystallites, speculated to arise from association of terthiophene side chains on the PTTEMA blocks. Since the DSC results reveal crystalline transitions in the $PTTEMA_{58}$-*b*-PS_{901} (18% PTTEMA) copolymer, we infer that this copolymer also has associated terthiophene domains that do not contribute significantly to the XRD pattern.

Figure 4 also shows XRD patterns for PTTEMA/PS homopolymer blends, measured for free-standing films rather than as powders. Thus, the intensity scales for the blend patterns differ from those for the copolymers. Bearing this in mind, the dominant peak in the pattern for the PTTEMA(60%)/PS(40%) blend clearly has a shape resembling those for PTTEMA homopolymer and the $PTTEMA_{58}$-*b*-PS_{136} (60% PTTEMA) copolymer. This is also true for the PTTEMA(40%)/PS(60%) blend. The latter also manifests the appearance of a peak near 2θ = 9° associated with the PS amorphous halo, which becomes quite prominent in the pattern for the PTTEMA(18%)/PS(82%) blend. The qualitative shapes of the peaks suggest that the blends also contain nanoscale domains resulting from the association of terthio-

DOI: 10.1021/am507751m
ACS Appl. Mater. Interfaces 2015, 7, 1967−1977

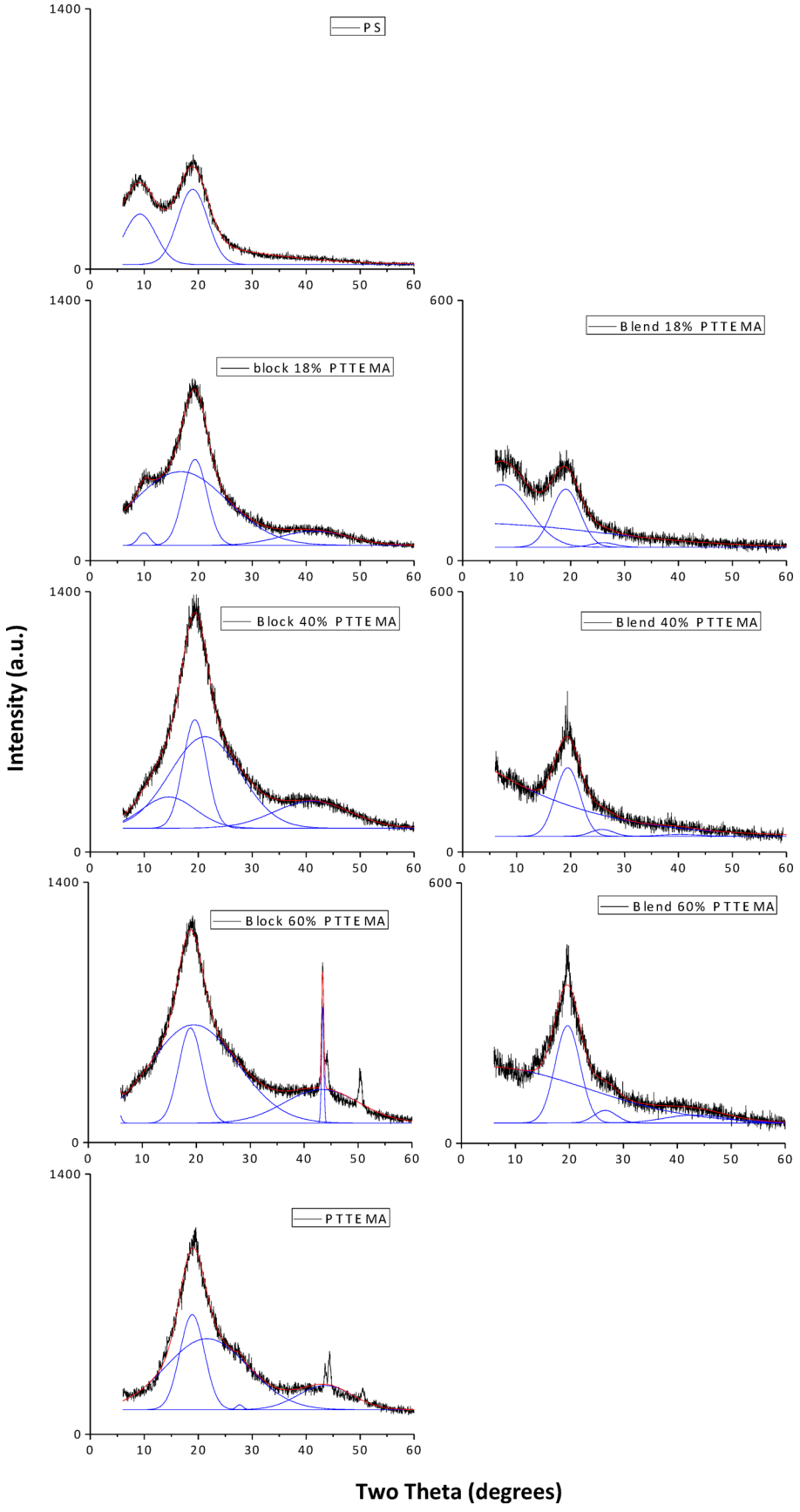

Figure 4. XRD patterns (black curves) for PTTEMA homopolymer, PS homopolymer, and PTTEMA-*b*-PS block copolymers (left column) and PTTEMA/PS polymer blends (right column, different intensity scales). Solid blue curves depict multiple peaks deconvoluted from the data. Solid red curve in each plot is the sum of the deconvoluted curves.

DOI: 10.1021/am507751m
ACS Appl. Mater. Interfaces 2015, 7, 1967−1977

phene side chains belonging to the PTTEMA homopolymer. However, interference from the PS amorphous halo makes it difficult to extract the crystallite domain size from the XRD data.

In our previous study of PTTEMA homopolymers,[38] AFM images failed to identify any features that could be ascribed to macro- or nanoscale phase separation. Likewise, AFM images of PTTEMA-*b*-PS copolymers did not reveal any evidence of organized structures that might be ascribed to phase separation. A representative image (Figure S7, Supporting Information) shows some small, faint features that could be sub-10 nm domains; however, this observation could be ascribed to a variety of artifacts common to AFM imaging.

3.3. Dielectric Properties. Figure 5 shows the frequency-dependent relative permittivities of PTTEMA-*b*-PS copolymers

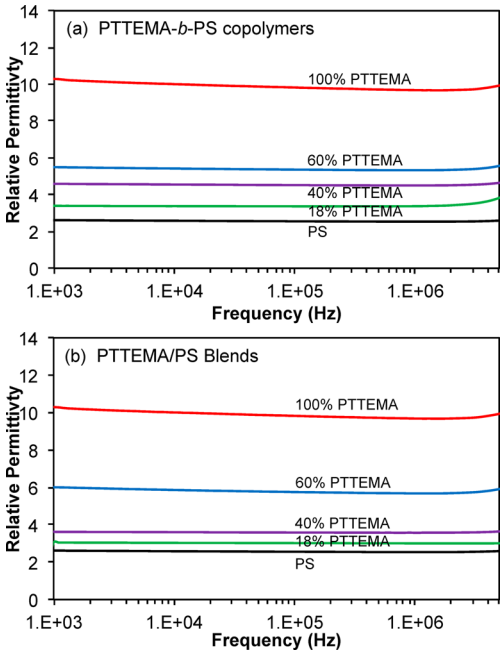

Figure 5. Relative permittivity as a function of frequency for (a) PTTEMA-*b*-PS copolymers and (b) PTTEMA/PS blends. PTTEMA weight percentages as indicated except for PS homopolymer.

and PTTEMA/PS blends. The relative permittivity of PS homopolymer is about 2.6 and nearly independent of frequency. The relative permittivity increases with PTTEMA wt % for both the PTTEMA-*b*-PS copolymers and the PTTEMA/PS blends. In all cases, the relative permittivities are virtually independent of frequency, which is remarkable compared to the significant frequency dependence of PVDF-based materials.[19−21,24,46,47]

Figure 6a more clearly shows the increase of relative permittivity with PTTEMA wt %; the increase is linear for the block copolymers and (approximately) quadratic for the blends. At lower PTTEMA weight percentages (18% and 40%), the block copolymers have higher relative permittivities than the polymer blends at the same PTTEMA wt %. However, the relative permittivities of the block copolymer and polymer blend with 60 wt % PTTEMA do not differ significantly. These observations may be rationalized in terms of polymer molecular architecture and subtle differences in crystalline domain size and distribution. With respect to architecture, previous work suggests that PTTEMA's terthiophene side chains associate to

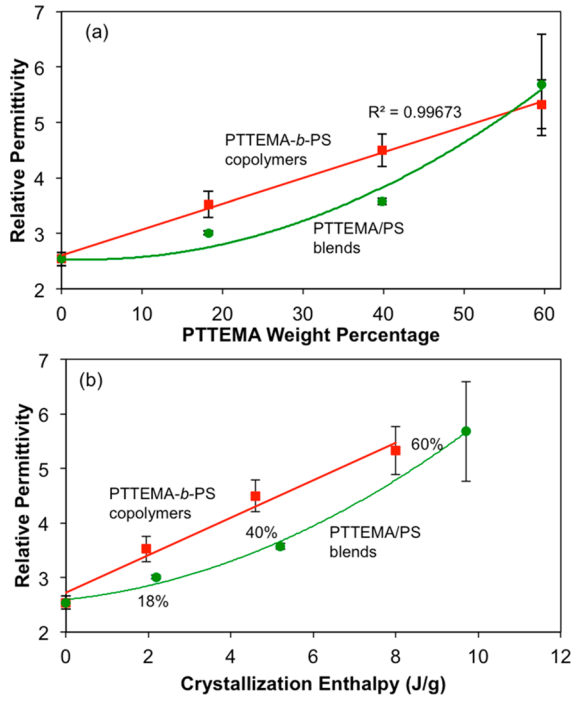

Figure 6. Dependence of relative permittivity on (a) PTTEMA weight percentage and (b) crystallization enthalpy. In both plots, the permittivity values for block copolymers and blends are fitted with linear and quadratic trend curves, respectively. Permittivity values were measured at a field frequency of 1.0 MHz. Error bars are 95% confidence intervals.

form small crystalline domains.[38] In PTTEMA-*b*-PS, each PTTEMA block is tethered to a PS block, with the latter having a larger molecular weight in all cases (Table 1). This creates a steric constraint that may limit the ability of PTTEMA blocks and their terthiophene side chains to associate. This constraint is absent in the PTTEMA/PS blends. Thus, the terthiophene side chains in the blends may associate to form a greater quantity of crystalline domains compared to the block copolymers, as indicated in Figure 3. At the same PTTEMA wt %, greater crystallinity in the PTTEMA/PS blends implies a lower number of somewhat larger domains. The lower density (number/volume) of polarizable domains may explain the lower relative permittivities of the 18% and 40% PTTEMA blends compared to the corresponding block copolymers (Figure 6a).

On the basis of DSC and XRD data (Figures 2−4), all of the PTTEMA-*b*-PS copolymers and PTTEMA/PS blends contain crystalline domains. In particular, the crystallization enthalpy data (Figure 3) show that the amount of crystallinity increases with PTTEMA wt %. Consequently, the relative permittivities of the block copolymers and polymer blends also increase with crystallization enthalpy (Figure 6b). The trends are again linear for the PTTEMA-*b*-PS copolymers and quadratic for the PTTEMA/PS blends. If the PS blocks are effective at isolating terthiophene domains associated with their tethered PTTEMA blocks then one might expect permittivity to increase linearly with the PTTEMA weight percentage, as illustrated schematically in Figure 7. More facile association of PTTEMA chains in the blends might lead to larger domains and a sublinear rate of permittivity increase with PTTEMA wt %.

Viewed another way, a PTTEMA-*b*-PS copolymer has greater permittivity than a PTTEMA/PS blend at the same level of

DOI: 10.1021/am507751m
ACS Appl. Mater. Interfaces 2015, 7, 1967−1977

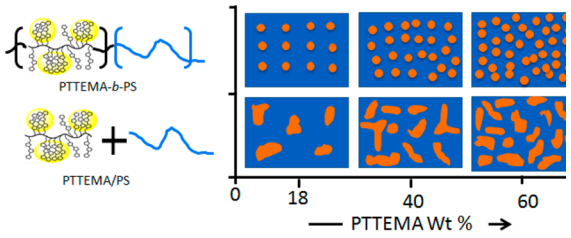

Figure 7. Schematic illustration of the proposed nanoscale structure in PTTEMA-*b*-PS copolymers and PTTEMA/PS blends with varying PTTEMA weight percentage.

crystallinity (as measured by crystallization enthalpy, Figure 6b). This implies that the size and/or nanoscale morphology of the crystalline domains influence the materials' relative permittivity. As suggested in Figure 7, we believe the nanoscale crystalline domains are smaller, more numerous, and better isolated in the PTTEMA-*b*-PS copolymer materials, resulting in higher polarization density and thus permittivity. However, at higher PTTEMA wt %, the advantage of relatively smaller domains in the block copolymers is nullified by percolation of adjacent domains, resulting in similar relative permittivities for the PTTEMA-*b*-PS block copolymers and PTTEMA/PS polymer blends.

The PTTEMA homopolymer has a loss tangent (tan δ) value less than 0.02 up to about 250 kHz but approaching 0.05 at 1.0 MHz field frequency (Figure 8). Compared to the PTTEMA

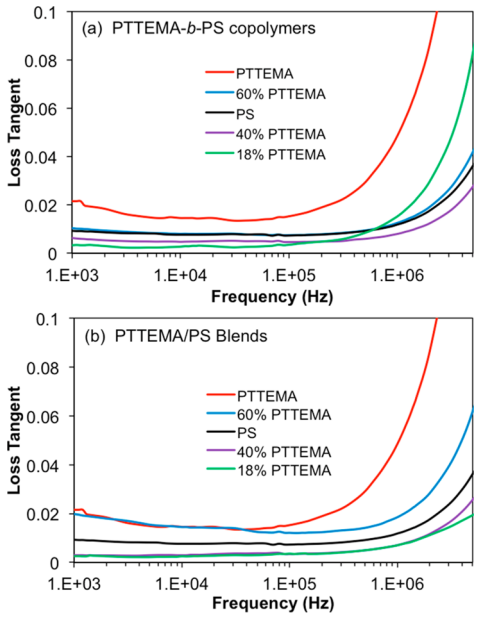

Figure 8. Loss tangent as a function of frequency for (a) PTTEMA-*b*-PS copolymers and (b) PTTEMA/PS blends. Legend order corresponds to the sequence of data curves in each plot.

homopolymer, all of the PTTEMA-*b*-PS copolymers and PTTEMA/PS blends exhibit lower loss tangent values that are nearly independent of field frequency over the 1.0 kHz to 1.0 MHz range. The tan δ values for the copolymers are below 0.01 nearly up to 1.0 MHz, as are the values for the blends with 18 and 40 wt % PTTEMA; the tan δ values for the 60 wt % PTTEMA blend are below 0.02 (Figure 8). The differences among the tan δ values for the copolymers and blends are probably not significant. Identical trends are observed in the data for specific conductivity (Figure S8, Supporting Information). The low, frequency-independent loss tangent values and low specific conductivities suggest that the dominant polarization mechanism does not involve configurational changes in polymer chains or crystallites. The permittivity, loss tangent, and conductivity results all support the view that the dominant polarization mechanism is localized electronic conduction within nanoscale terthiophene-rich crystalline domains.

Polarization testing characterizes the dielectric behavior of materials at higher applied electric fields than impedance measurements. Figure 9 shows typical polarization ($D-E$)

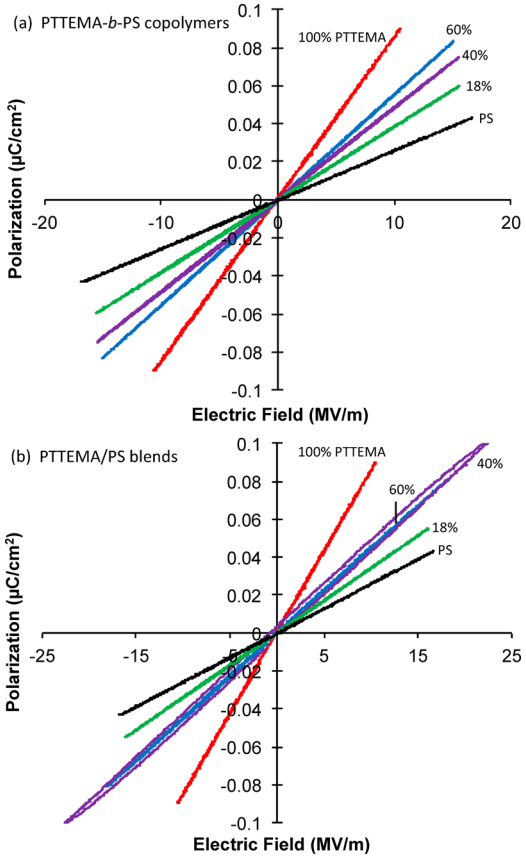

Figure 9. Polarization ($D-E$) loops for (a) PTTEMA-*b*-PS copolymers and (b) PTTEMA/PS blends. Curve labels denote the PTTEMA wt % (except PS homopolymer).

loops for PTTEMA-*b*-PS copolymers and PTTEMA/PS blends. All of these materials exhibit linear polarization behavior when the maximum applied electric field is relatively low (<25 MV/m). At a fixed field strength, the polarization increases with PTTEMA wt % for both copolymers and blends. The linear polarization behavior and low hysteresis observed for both the copolymers and the blends indicates low levels of energy dissipation, consistent with the low loss tangent values from impedance measurements (Figure 8).

Integration of the $D-E$ loop (as described earlier) gives the stored energy density as a function of the maximum electric field strength applied during the polarization test (Figure 10). The state of the film sample (freestanding versus supported on an aluminum pan) appears to influence these results. Films of PTTEMA homopolymer, PTTEMA-*b*-PS copolymers, and 60 wt % PTTEMA/PS blend were all brittle and difficult to peel

DOI: 10.1021/am507751m
ACS Appl. Mater. Interfaces 2015, 7, 1967−1977

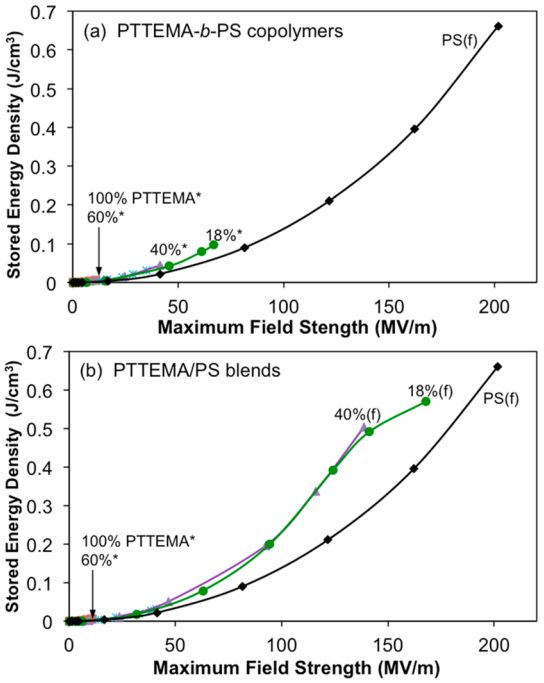

Figure 10. Stored energy density as a function of maximum electric field strength for (a) PTTEMA-*b*-PS copolymers and (b) PTTEMA/PS blends. Curve labels denote the PTTEMA wt % (except PS homopolymer); label symbols (* and f) denote films supported on aluminum pans and freestanding films, respectively.

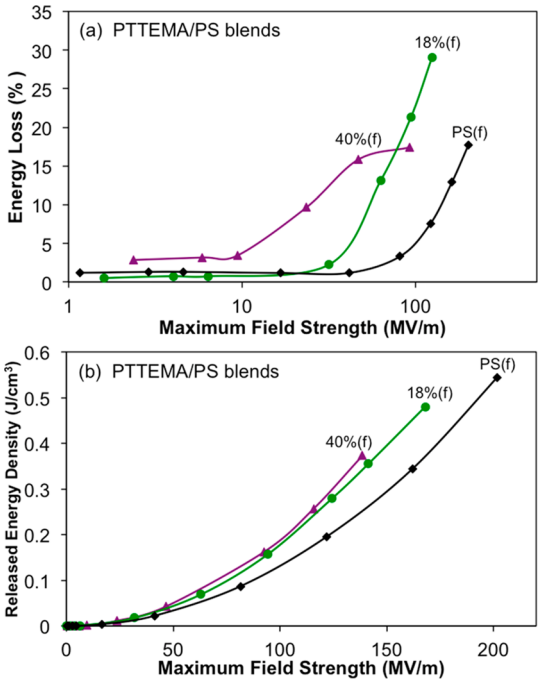

Figure 11. (a) Energy loss as a function of maximum electric field strength (logarithmic scale), and (b) released energy density as a function of maximum electric field strength for freestanding films of PS homopolymer and two PTTEMA/PS blends (18 and 40 wt %).

from various casting surfaces, so samples for polarization testing remained supported on aluminum pans. All of the film samples supported on Al pans exhibited dielectric breakdown at relatively low field strength values and thus did not manifest large values of stored energy density (Figure 10a and 10b). In contrast, PS homopolymer and PTTEMA/PS blends containing 18 and 40 wt % PTTEMA could be peeled from casting surfaces and tested as freestanding films. These films could be polarized to relatively high field strengths and therefore manifested higher stored energy densities (Figure 10b).

The reasons for these observations are uncertain and will require more testing to elucidate. For now, we speculate that large electromechanical stresses generated by the high electric fields in the Al-supported films may result in structural changes accompanied by premature dielectric breakdown. This rationalization is supported by polarization data for PTTEMA homopolymers with varying molecular weight. Higher molecular weight $PTTEMA_{92}$ can be polarized[48] to a greater maximum field strength than $PTTEMA_{58}$ (Figure S9, Supporting Information). Assuming that $PTTEMA_{92}$ has greater entanglement and elastic modulus than $PTTEMA_{58}$, the former would be able to withstand higher mechanical stresses arising from the applied electric field.

Considering only freestanding films, the stored energy densities for 18 and 40 wt % PTTEMA/PS films are significantly higher than that for the PS homopolymer film (Figure 10b). Thus, the presence of PTTEMA as a minority component in the blend enhances dielectric energy storage due to the presence of the higher polarizability terthiophene domains (Figure 7). The data for percentage energy loss (Figure 11a) show that PS and PTTEMA/PS blends have nearly constant, low values of energy loss at low applied field strengths, but the losses begin to increase significantly near a critical value of field strength that decreases with increasing PTTEMA content. Physically, as the density of terthiophene domains increases (Figure 7), we expect increasing leakage of electronic current across the PS that separates the domains, resulting in the shift of the upturn in energy loss to lower field strength.

Despite the significant energy loss at higher field strength, the recovered energy densities for 18 and 40 wt % PTTEMA/PS films are still higher than that for PS homopolymer film (Figure 11b). Near the breakdown strength for the 18 wt % PTTEMA/PS film (ca. 160 MV/m), its recovered energy density is about 40% greater than the PS film. For the 40 wt % PTTEMA/PS film (breakdown at ca. 138 MV/m), its recovered energy density is about 46% greater than the PS film. These results demonstrate that the recovered energy density in PS homopolymer films can be enhanced by the addition of a small fraction of PTTEMA homopolymer. However, this is accompanied by an increase in the percentage energy loss, probably due to current leakage between terthiophene domains.

4. CONCLUSIONS

The promising dielectric properties of π-conjugated terthiophene-containing polymers have motivated our efforts to better understand the polarization mechanisms in these materials. To explore this topic, we prepared a series of diblock copolymers made of polystyrene and terthiophene-containing methacrylate (PTTEMA-*b*-PS) with varying PTTEMA content, as well as polymer blends of PTTEMA/PS with the same weight fractions of PTTEMA.

DSC and XRD results reveal the presence of crystallinity in all PTTEMA-*b*-PS copolymers and PTTEMA/PS blends, which we attribute to nanoscale association of terthiophene side groups from the PTTEMA component. The materials'

DOI: 10.1021/am507751m
ACS Appl. Mater. Interfaces 2015, 7, 1967−1977

relative permittivities increase with PTTEMA wt %, as might be expected. At the same PTTEMA wt % or at the same degree of crystallinity (as measured by crystallization enthalpy), PTTEMA-*b*-PS copolymer has a higher permittivity than the corresponding PTTEMA/PS blend. This can be rationalized by the steric constraints created by PS blocks, which tend to reduce association of the tethered PTTEMA blocks in PTTEMA-*b*-PS copolymer films. In contrast, PTTEMA chains tend to associate more when less constrained in PTTEMA/PS blends. When PTTEMA is the majority component (content >60 wt %), these differences become unimportant and copolymers and blends have similar dielectric properties.

Polarization testing shows that PTTEMA-*b*-PS copolymers and PTTEMA/PS blends have linear polarization behavior and low hysteresis at electric fields up to about 10 MV/m. However, at higher electric fields, films supported on Al metal undergo premature dielectric breakdown, possibly due to field-induced mechanical stresses and concomitant deformation. Blending up to 40 wt % PTTEMA homopolymer with PS homopolymer leads to freestanding films that can be polarized to maximum field strengths comparable to pure PS. The addition of PTTEMA increases energy losses that are probably associated with current leakage between nearby terthiophene-rich domains. Nonetheless, adding PTTEMA to PS can result in recovered energy density values approaching 0.5 J/cm^3 (18 wt % PTTEMA/PS), a value 40% greater than that found for pure PS at the same maximum applied electric field.

■ ASSOCIATED CONTENT

Supporting Information

Additional NMR spectra for $PTTEMA_{58}$ homopolymer and various PTTEMA-*b*-PS copolymers; GPC characterization results for PTTEMA-*b*-PS copolymers; specific conductivity results for PTTEMA-*b*-PS copolymers and PTTEMA/PS blends; stored energy density and energy loss results for two PTTEMA homopolymers with differing molecular weights. This material is available free of charge via the Internet at http://pubs.acs.org.

■ AUTHOR INFORMATION

Corresponding Author

*E-mail: Ploehn@mailbox.sc.edu.

Notes

The authors declare no competing financial interest.

■ ACKNOWLEDGMENTS

This work was supported by the Office of Naval Research (award N000141110191) and SC NASA EPSCoR (award 22-NE-USC_Tang). We thank Prof. Hans-Conrad zur Loye and his research group for assistance with XRD measurements.

■ REFERENCES

(1) Barber, P.; Balasubramanian, S.; Anguchamy, Y.; Gong, S.; Wibowo, A.; Gao, H.; Ploehn, H. J.; Zur Loye, H.-C. Polymer Composite and Nanocomposite Dielectric Materials for Pulse Power Energy Storage. *Materials* **2009**, *2*, 1697−1733.

(2) Cao, Y.; Irwin, P. C.; Younsi, K. The Future of Nanodielectrics in the Electrical Power Industry. *IEEE Trans. Dielectr. Electr. Insul.* **2004**, *11*, 797−807.

(3) Nalwa, H. S. *Handbook of Low and High Dielectric Constant Materials and Their Applications*; Academic Press: London, U.K., 1999.

(4) Osaka, T.; Datta, M. *Energy Storage Systems in Electronics*; Gordon and Breach: Amsterdam, The Netherlands, 2001.

(5) Barshaw, E.; White, J.; Chait, M.; Cornette, J.; Bustamante, J.; Folli, F.; Biltchick, D.; Borelli, G.; Picci, G.; Rabuffi, M. High Energy Density (HED) Biaxially-Oriented Poly-Propylene (BOPP) Capacitors for Pulse Power Applications. *IEEE Trans. Magn.* **2007**, *43*, 223−225.

(6) Dang, Z.-M.; Yuan, J.-K.; Zha, J.-W.; Zhou, T.; Li, S.-T.; Hu, G.-H. Fundamentals, Processes and Applications of High-Permittivity Polymer−Matrix Composites. *Prog. Mater. Sci.* **2012**, *57*, 660−723.

(7) Nelson, J. K. *Dielectric Polymer Nanocomposites*; Springer: New York, 2010.

(8) Tanaka, T. Dielectric Nanocomposites with Insulating Properties. *IEEE Trans. Dielectr. Insul.* **2005**, *12*, 914−928.

(9) Wang, Q.; Zhu, L. Polymer Nanocomposites for Electrical Energy Storage. *J. Polym. Sci., Part B: Polym. Phys.* **2011**, *49*, 1421−1429.

(10) Huang, X.; Jiang, P. Core−Shell Structured High-k Polymer Nanocomposites for Energy Storage and Dielectric Applications. *Adv. Mater.* **2014**, DOI: 10.1002/adma.201401310.

(11) Zhu, L. Exploring Strategies for High Dielectric Constant and Low Loss Polymer Dielectrics. *J. Phys. Chem. Lett.* **2014**, *5*, 3677−3687.

(12) Chu, B.; Zhou, X.; Ren, K.; Neese, B.; Lin, M.; Wang, Q.; Bauer, F.; Zhang, Q. A Dielectric Polymer with High Electric Energy Density and Fast Discharge Speed. *Science* **2006**, *313* (5785), 334−336.

(13) Claude, J.; Lu, Y.; Li, K.; Wang, Q. Electrical Storage in Poly (vinylidene fluoride) based Ferroelectric Polymers: Correlating Polymer Structure to Electrical Breakdown Strength. *Chem. Mater.* **2008**, *20*, 2078−2080.

(14) Guan, F.; Pan, J.; Wang, J.; Wang, Q.; Zhu, L. Crystal Orientation Effect on Electric Energy Storage in Poly (vinylidene fluoride-co-hexafluoropropylene) Copolymers. *Macromolecules* **2009**, *43*, 384−392.

(15) Wang, Z.; Zhang, Z.; Chung, T. C. M. High Dielectric VDF/TrFE/CTFE Terpolymers Prepared by Hydrogenation of VDF/CTFE Copolymers: Synthesis and Characterization. *Macromolecules* **2006**, *39*, 4268−4271.

(16) Zhang, Z.; Chung, T. C. M. The Structure−Property Relationship of Poly(vinylidene difluoride)-Based Polymers with Energy Storage and Loss under Applied Electric Fields. *Macromolecules* **2007**, *40*, 9391−9397.

(17) Zhang, Z.; Chung, T. C. M. Study of VDF/TrFE/CTFE Terpolymers for High Pulsed Capacitor with High Energy Density and Low Energy Loss. *Macromolecules* **2007**, *40*, 783−785.

(18) Zhang, Z.; Meng, Q.; Chung, T. Energy Storage Study of Ferroelectric Poly (vinylidene fluoride-trifluoroethylene-chlorotrifluoroethylene) Terpolymers. *Polymer* **2009**, *50*, 707−715.

(19) Bornand, V.; Vacher, C.; Collet, A.; Papet, P. Interest of Binary PMMA/P(VDF-TrFE) Blend Thin Films. *Mater. Chem. Phys.* **2009**, *117*, 169−172.

(20) Chu, B.; Neese, B.; Lin, M.; Lu, S.-g.; Zhang, Q. Enhancement of Dielectric Energy Density in the Poly (vinylidene fluoride)-based Terpolymer/Copolymer Blends. *Appl. Phys. Lett.* **2008**, *93*, 152903−152903−3.

(21) Li, R.; Xiong, C.; Kuang, D.; Dong, L.; Lei, Y.; Yao, J.; Jiang, M.; Li, L. Polyamide 11/Poly (vinylidene fluoride) Blends as Novel Flexible Materials for Capacitors. *Macromol. Rapid Commun.* **2008**, *29*, 1449−1454.

(22) Meng, Q.; Li, W.; Zheng, Y.; Zhang, Z. Effect of Poly (methyl methacrylate) Addition on the Dielectric and Energy Storage Properties of Poly (vinylidene fluoride). *J. Appl. Polym. Sci.* **2010**, *116*, 2674−2684.

(23) Rahimabady, M.; Yao, K.; Arabnejad, S.; Lu, L.; Shim, V. P.; Chet, D. C. W. Intermolecular Interactions and High Dielectric Energy Storage Density in Poly (vinylidene fluoride-hexafluoropropylene)/Poly (vinylidene fluoride) Blend Thin Films. *Appl. Phys. Lett.* **2012**, *100*, 252907.

(24) Wu, S.; Lin, M.; Lu, S.; Zhu, L.; Zhang, Q. Polar-Fluoropolymer Blends with Tailored Nanostructures for High Energy Density Low Loss Capacitor Applications. *Appl. Phys. Lett.* **2011**, *99*, 132901.

DOI: 10.1021/am507751m
ACS Appl. Mater. Interfaces 2015, 7, 1967−1977

(25) Zhang, S.; Neese, B.; Ren, K.; Chu, B.; Zhang, Q. Microstructure and Electromechanical Responses in Semicrystalline Ferroelectric Relaxor Polymer Blends. *J. Appl. Phys.* **2006**, *100*, 044113.
(26) Chwang, C. P.; Liu, C. D.; Huang, S. W.; Chao, D. Y.; Lee, S. N. Synthesis and Characterization of High Dielectric Constant Polyaniline/Polyurethane Blends. *Synth. Met.* **2004**, *142*, 275−281.
(27) Guo, M.; Hayakawa, T.; Kakimoto, M.; Goodson, T. Organic Macromolecular High Dielectric Constant Materials: Synthesis, Characterization, and Applications. *J. Phys. Chem. B* **2011**, *115*, 13419−13432.
(28) Huang, C.; Zhang, Q.; Su, J. High-Dielectric-Constant All-Polymer Percolative Composites. *Appl. Phys. Lett.* **2003**, *82*, 3502−3504.
(29) Huang, C.; Zhang, Q. M. Enhanced Dielectric and Electromechanical Responses in High Dielectric Constant All-Polymer Percolative Composites. *Adv. Funct. Mater.* **2004**, *14*, 501−506.
(30) Huang, C.; Zhang, Q. M. Fully Functionalized High-Dielectric-Constant Nanophase Polymers with High Electromechanical Response. *Adv. Mater.* **2005**, *17*, 1153−1158.
(31) Huang, C.; Zhang, Q. M.; deBotton, G.; Bhattacharya, K. All-organic Dielectric-Percolative Three-Component Composite Materials with High Electromechanical Response. *Appl. Phys. Lett.* **2004**, *84*, 4391−4393.
(32) Molberg, M.; Crespy, D.; Rupper, P.; Nueesch, F.; Manson, J.-A. E.; Loewe, C.; Opris, D. M. High Breakdown Field Dielectric Elastomer Actuators Using Encapsulated Polyaniline as High Dielectric Constant Filler. *Adv. Funct. Mater.* **2010**, *20*, 3280−3291.
(33) Zhang, Q. M.; Li, H. F.; Poh, M.; Xia, F.; Cheng, Z. Y.; Xu, H. S.; Huang, C. An all-organic Composite Actuator Material with a High Dielectric Constant. *Nature* **2002**, *419*, 284−287.
(34) Hardy, C. G.; Islam, M.; Gonzalez-Delozier, D.; Ploehn, H. J.; Tang, C. Oligoaniline-Containing Supramolecular Block Copolymer Nanodielectric Materials. *Macromol. Rapid Commun.* **2012**, *33*, 791−797.
(35) Hardy, C. G.; Islam, M. S.; Gonzalez-Delozier, D.; Morgan, J. E.; Cash, B.; Benicewicz, B. C.; Ploehn, H. J.; Tang, C. Converting an Electrical Insulator into a Dielectric Capacitor: End-Capping Polystyrene with Oligoaniline. *Chem. Mater.* **2013**, *25*, 799−807.
(36) McCullough, L. A.; Dufour, B.; Matyjaszewski, K. Polyaniline and Polypyrrole Templated on Self-Assembled Acidic Block Copolymers. *Macromolecules* **2009**, *42*, 8129−8137.
(37) McCullough, L. A.; Dufour, B.; Tang, C.; Zhang, R.; Kowalewski, T.; Matyjaszewski, K. Templating Conducting Polymers via Self-Assembly of Block Copolymers and Supramolecular Recognition. *Macromolecules* **2007**, *40*, 7745−7747.
(38) Qiao, Y.; Islam, M. S.; Han, K.; Leonhardt, E.; Zhang, J.; Wang, Q.; Ploehn, H. J.; Tang, C. Polymers Containing Highly Polarizable Conjugated Side Chains as High-Performance All-Organic Nanodielectric Materials. *Adv. Funct. Mater.* **2013**, *23*, 5638−5646.
(39) Hardy, C. G. Functional Block Copolymers For Applications In Advanced Materials, Energy Storage, and Lithography. Ph.D. Thesis, University of South Carolina, 2013.
(40) Li, J. J.; Khanchaitit, P.; Han, K.; Wang, Q. New Route Toward High-Energy-Density Nanocomposites Based on Chain-End Functionalized Ferroelectric Polymers. *Chem. Mater.* **2010**, *22*, 5350−5357.
(41) Patterson, A. The Scherrer Formula for X-Ray Particle Size Determination. *Phys. Rev.* **1939**, *56* (10), 978.
(42) Scherrer, A.; Gottingen, N. *Elements of X-Ray Diffraction*. Addision-Wesley: Reading, MA, 1918.
(43) Zhu, L.; Calhoun, B. H.; Ge, Q.; Quirk, R. P.; Cheng, S. Z. D.; Thomas, E. L.; Hsiao, B. S.; Yeh, F.; Liu, L.; Lotz, B. Initial-Stage Growth Controlled Crystal Orientations in Nanoconfined Lamellae of a Self-Assembled Crystalline−Amorphous Diblock Copolymer. *Macromolecules* **2001**, *34*, 1244−1251.
(44) Kilian, H. G.; Boueke, K. Röntgenographische Strukturanalyse von Amorphem Polystyrol. VI. *J. Polym. Sci.* **1962**, *58*, 311−333.
(45) Tawansi, A.; El-Khodary, A.; Oraby, A.; Youssef, A. Effect of $AgNO_3$-$MnCl_2$ Mixed Fillers on The Physical Properties of Polystyrene Films. *J. Appl. Polym. Sci.* **2005**, *95*, 1333−1341.
(46) Faria, L. O.; Moreira, R. L. Dielectric Behavior of P(VDF-TrFE)/PMMA Blends. *J. Polym. Sci., Part B: Polym. Phys.* **1999**, *37*, 2996−3002.
(47) Gregorio, R.; Malmonge, L. F.; Ferreira, G. F. L.; dos Santos, W. N.; Mattoso, L. H. C. Dielectric Behavior of PVDF/POMA Blends that Have a Low Doped POMA Content. *J. Appl. Polym. Sci.* **2003**, *87*, 752−758.
(48) Qiao, Y.; Islam, M. S.; Wang, L.; Yan, Y.; Zhang, J.; Benicewicz, B. C.; Ploehn, H. J.; Tang, C. Thiophene Polymer-Grafted Barium Titanate Nanoparticles toward Nanodielectric Composites. *Chem. Mater.* **2014**, *26*, 5319−5326.

DOI: 10.1021/am507751m
ACS Appl. Mater. Interfaces 2015, 7, 1967−1977